Results in Surfaces and Interfaces 24 (2026) 100850

Contents lists available at ScienceDirect

Results in Surfaces and Interfaces

journal homepage: www.elsevier.com/locate/rsurfi

# Effects of boriding and niobium carbide coating on the microstructure, hardness, and tribocorrosion properties of Vanadis 6 tool steel

Venu Yarasu [a,*], Bojan Podgornik [a], Tadeja Kosec [b], Peter Jurči [c], Ali Günen [d], Peter Orihel [c], Sabri Alkan [e]

[a] Institute of Metals and Technology, Lepi pot 11, Ljubljana, 1000, Slovenia
[b] Slovenian National Building and Civil Engineering Institute, Dimičeva 12, Ljubljana, 1000, Slovenia
[c] Faculty of Materials Technology based in Trnava, Slovak University of Technology in Bratislava, Slovakia
[d] Faculty of Engineering and Natural Sciences, İskenderun Technical University, İskenderun, 31200, Türkiye
[e] Faculty of Maritime, Bandırma Onyedi Eylül University, Balıkesir, 10200, Türkiye

ARTICLE INFO

*Keywords:*
Vanadis 6 steel
Surface modification
Microstructure
Hardness
Tribocorrosion

ABSTRACT

Vanadis 6 (V6) cold work tool steel is widely used in cold forming applications due to its high wear resistance and toughness. However, tribocorrosion remains a major challenge in aggressive manufacturing conditions limiting the tool life. This study investigates the effect of boride and niobium (NbC) coatings on the microstructure, hardness, and tribocorrosion properties of V6 tool steel. Both uncoated and coated samples were tested in 0.1 M NaCl (pH 7), 0.001 M NaOH (pH 11), and Na-tetraborate (pH 10) solutions. The microstructural changes and phase analysis were examined via a scanning electron microscope coupled with energy-dispersive spectroscopy (SEM-EDS) and X-ray diffraction, while the hardness was evaluated using Vickers microhardness (HV). The tribocorrosion tests were performed by monitoring the open circuit potential (OCP) with a reciprocating pin-on-disk configuration. Wear surface analysis was conducted using 3D confocal microscopy, Raman spectroscopy, and SEM-EDS techniques. The findings indicated that the application of coatings enhanced the surface hardness from 710 $HV_{30}$ to 2000 $HV_{0.1}$ and 1550 $HV_{0.1}$ for boride and NbC coatings, respectively. During the tribocorrosion experiments, the samples coated with NbC and borides consistently displayed the highest open-circuit potential (OCP) in all the solutions. These results confirm that both NbC and borides improved the tribological and corrosion resistance of Vanadis 6 steel, with the NbC coating offering a more effective and stable protective layer. The outcome of this study emphasizes the critical role of coatings and the appropriate choice of electrolytes for comparative evaluation in the tribocorrosion behavior of cold work tool steels.

## 1. Introduction

The application of cold work tool steels, such as Vanadis 6 (V6), which is produced through powder metallurgy, is widely used in high-demand manufacturing processes, particularly in high-speed stamping, drawing, and complex cold forming. In addition to these primary uses, such materials also find applications in mining, concrete processing, and the manufacturing of stationery products. These materials are chosen for their ideal combination of high strength, fracture toughness, and remarkable wear resistance. The unique performance attributes are attained through heat treatment that carefully oversees microstructure, which is defined by a significant presence of hard vanadium carbides (VC) and martensite [1–4]. Despite these inherent mechanical advantages, the operational lifespan of cold work tool steels is often reduced by complex surface degradation phenomena [5,6]. Tribocorrosion, the combined effect of mechanical wear and corrosion, is a major cause of material failure in harsh industrial settings that frequently involve coolants, cutting fluids, or corrosive atmospheric moisture. The combined effects of these processes can cause material loss that is considerably more severe than the mere sum of individual wear and corrosion, underscoring the importance of implementing proactive surface modification strategies [7].

The integration of cryogenic treatment and surface engineering, primarily through the application of advanced protective coatings, represents the most effective method to reduce the tribocorrosion challenge associated with many metals [8–11]. Among the most

* Corresponding author.
*E-mail address:* venu.yarasu@imt.si (V. Yarasu).

https://doi.org/10.1016/j.rsurfi.2026.100850
Received 2 February 2026; Received in revised form 13 April 2026; Accepted 21 May 2026
Available online 22 May 2026

promising surface treatments are thermochemical diffusion processes (TCD), specifically boriding and the development of niobium carbide (NbC) coatings, which are acknowledged to greatly improve surface hardness and chemical inertness [12,13]. Among these two techniques, boriding is more widely adopted due to its relative simplicity and lower production costs, largely stemming from the broader availability of the chemical agents required for the process. The process of TCD involves the heating of the steel substrate in a powder-pack or salt bath containing the desired element (boron or niobium) and a carbon donor. This procedure leads to the development of a hard and dense compound layer on the surface [14]. For boriding, the resulting layer on tool steels is predominantly composed of iron borides (FeB and $Fe_2B$), often with an increased concentration of newly formed carbides in the transition zone due to the diffusion of carbon from the steel matrix [15]. Studies on V6 steel have confirmed the successful formation of these boride layers, which significantly enhance surface hardness [16,17]. Similarly, NbC coatings produced by TCD on various steels, including AISI D2, exhibit remarkable hardness (up to 2700 HV) and strong adherence to the substrate, primarily due to the low-volume expansion during their formation [6,18].

The central hypothesis across the literature is that the hard coatings can provide superior mechanical wear and tribocorrosion resistance compared to the uncoated substrate. The few studies specifically addressing AISI D2 and D3 steels, such as those by Mehmet and Günen, suggest that both borided and NbC-treated surfaces exhibit significantly reduced material loss under tribocorrosion conditions [19,20]. The superior performance of the coated steels is attributed to two primary factors. First comes from the mechanical barrier as the extreme hardness of the boride- and NbC-layers reduces the wear component of the degradation by limiting plastic deformation and material removal during sliding contact [21]. Second, the electrochemical inertness: comes from the ceramic nature of the coatings providing a passive barrier that inhibits the electrochemical dissolution of the underlying steel [22]. However, a critical limitation emerges in the literature when comparing the two coatings. While NbC coatings are often cited for their exceptional chemical stability and low friction coefficient [20], borided layers can sometimes suffer from micro-cracking or porosity, which, when exposed by wear, can accelerate galvanic corrosion of the steel substrate [23]. Beyond tribocorrosion behavior, the functional performance of cold-work tool steels also depends critically on maintaining sufficient toughness. Toughness is the measure of material's resistance to the initiation and propagation of brittle fracture. This is commonly evaluated using Charpy impact testing or flexural strength methods. Recent experimental data show that V6 steel exhibits a Charpy impact toughness of $44.5 \pm 8.4$ J/cm$^2$ [17]. However, the formation of a borided layer drastically reduces this value to approximately 2.0 J/cm$^2$, indicating a severe embrittlement effect. In contrast, NbC layers induce a moderate reduction, typically only 20-40%. The tribocorrosion mechanism in both cases involves a synergistic effect where the mechanical removal of the passive oxide film during sliding exposes the active metal surface to the corrosive electrolyte, leading to accelerated material loss [5]. For coated AISI D2 steel, the failure mode shifts from simple adhesive wear-corrosion of the uncoated steel to the progressive mechanical fracture and electrochemical dissolution of the coating itself [15].

The choice of electrolyte is perhaps the most critical, yet least standardized variable in tribocorrosion testing. The literature reveals that NaCl, NaOH, and Na-tetraborate solutions each simulate distinct service environments and induce fundamentally different degradation mechanisms. The 3.5 wt% NaCl solution is the de facto standard for simulating marine, biological, or general chloride-rich environments [24,25]. It can be used, for instance, for testing tools or components intended to operate in seawater or in close vicinity to the sea coast [26]. Chloride ions ($Cl^-$) are known to be highly aggressive, effectively penetrating and destabilizing the passive oxide layer on steel surfaces [27]. NaCl is highly suitable for testing the worst-case scenario performance of coated materials. Studies using NaCl consistently show that the synergistic effect is maximized, as the wear track is immediately depassivated by the chloride ions, leading to high corrosion currents and rapid material loss [28]. The limitation of NaCl is that it may be too aggressive, potentially masking subtle differences in coating quality or performance by forcing rapid, catastrophic failure [5].

NaOH solutions are used to simulate highly alkaline (pH $>$ 10.5) industrial environments. In the case of tool-steel applications, this may represent, for instance, the wood industry, as worked wood contains 20-30% of lignin with a pH of up to 10 [29]. In alkaline media, steel surfaces tend to form a more stable, thicker passive film than in neutral or acidic solutions. Tribocorrosion testing in NaOH is therefore excellent for evaluating the mechanical stability of the boride and NbC coatings, as the corrosion component is minimized. The primary degradation pathway shifts to the mechanical removal of the coating, with the electrolyte acting more as a lubricant or a medium for mild chemical interaction rather than a strong corrodent [30–32]. This environment is crucial for separating the wear and corrosion components of the synergy.

Sodium tetraborate is used to simulate highly alkaline concrete environments. It may be used, for instance, for testing the corrosion resistance of reinforcing steels (rebars) [33]. But a potential use in corrosion testing of coated tools in civil engineering can also be expected. Borate ions are recognized corrosion inhibitors for steel, known to promote passive film formation [34]. The use of borax-based electrolytes in tribological and electrochemical studies, their role as a standalone medium for tribocorrosion testing of tool steels remains underexplored in the literature. This medium offers a controlled, inhibited environment that simulates industrial coolants or lubricants, allowing researchers to isolate the tribological behavior of coating's conditions where electrochemical degradation is minimized [35]. Such testing facilitates evaluation of repassivation kinetics and long-term performance in non-aggressive wear regimes.

The existing literature provides a basis for understanding the tribological and corrosion behavior of surface-modified tool steels, particularly those treated with boriding and NbC coatings produced through the TRD technique. Moreover, various studies [5,12] show that both treatments improve resistance to mechanical wear and corrosion when compared with uncoated substrates, largely due to the formation of hard, chemically stable surface layers that slow or suppress degradation process. Despite this progress, important gaps remain that limit the development of standardized tribocorrosion testing approaches. Although tribocorrosion behavior has been reported for borided V6 steel [36] and NbC-coated cold-work tool steels such as D3 [20], the literature lacks a direct, systematic comparison of borided and NbC-treated V6 steel evaluated under identical experimental conditions. Additionally, the high vanadium and chromium content of V6 steel could strongly influence the diffusion layer formation and properties of both the boride and NbC coatings potentially altering the expected mechanical stability and electrochemical performance. Furthermore, while the use of NaCl and NaOH electrolytes is well-documented in tribocorrosion research, the application of Na-tetraborate remains unexplored. Consequently, there is a lack of systematic studies evaluating the influence of these three electrolytes on the tribocorrosion behavior of coated tool steels [28,37], which hinders the development of a unified testing protocol capable of capturing diverse electrochemical environments. Although V6 is commonly used under lubricated forming conditions, the modern industrial trends toward green manufacturing may often replace oil-based lubricants with aqueous solutions or synthetic fluids that may influence the corrosion properties [38,39]. At the same time, the need to maintain acceptable toughness in cold-work tool steels further underscores the importance of comparing the two coating systems, as recent findings indicate that NbC-coated V6 retains significantly higher impact toughness than its borided counterpart.

The above overview provides the basis for defining the main goals of the investigation, which are: (i) to conduct a mechanistic assessment of early tribocorrosion response of borided and NbC-coated V6 steel in

NaCl, NaOH, and Na-tetraborate solutions where synergy effects may become most significant; (ii) elaboration of the first comprehensive, comparative investigation of borided and NbC-treated tool steel under combined wear and electrochemical attack; (iii) providing essential data for establishing a more coherent and scientifically grounded tribocorrosion testing framework; and (iv) determination of the possible substitution of boride coatings by NbC coatings in tribocorrosion protection of tools in practice, as this would benefit from the much lower detrimental effect of NbC on tool toughness.

## 2. Materials and methods

This study utilized commercially available Vanadis 6 (V6) cold-work tool steel produced through powder metallurgy as the substrate material. The measured chemical composition of the steel obtained by the optical emission spectroscopy analysis is provided in Table 1. From the soft annealed state, rectangular plate specimens were machined to dimensions of 51 × 15 × 5 mm. These specimens were divided into three groups: 3 (uncoated), 3B (Borided), and 3N (NbC-coated).

Further, boriding was applied to the 3B samples using a solid-state pack method. This process utilized a commercial boriding mixture containing $B_4C$ and active agents. The samples were embedded in the mixture, sealed in a stainless-steel container to prevent oxidation, and then subjected to heat treatment at 1050 °C for 10 h. The resulting coating thickness was maintained at approximately 100 μm. In parallel, NbC coatings were deposited on 3N samples using a powder mixture with a specified composition of 35% ferroniobium, 60% $Al_2O_3$, and 5% $NH_4Cl$ by weight. These samples were also placed in stainless-steel containers, and the coating process was conducted at 1000 °C for 6 h. The thickness of the NbC coating was controlled to approximately 15 μm. It should be noted that the boride and NbC coatings differ in thickness due to the nature of their respective thermos reactive diffusion (TRD) process. Since the aim of this study is to compare the mechanistic tribocorrosion response of these two coatings rather than their absolute lifetime durability, the thickness difference is intrinsic to the comparison and does not affect the validity of the mechanistic evaluation. After completion of the coating procedures, all samples were removed from the furnace and allowed to cool to room temperature in air. Subsequently, all the samples underwent conventional heat treatment (CHT). The CHT process involved austenitizing at 1050 °C for 30 min, followed by nitrogen gas quenching at 5 bar pressure to room temperature. After CHT, double tempering was performed at 530 °C for 2 h. Uncoated, polished samples were examined using standard metallographic techniques to establish baseline microstructural characteristics.

Following the heat treatment process, all specimens underwent standard metallographic preparation for microstructural evaluation including mounting of cross-sectional surfaces, sequential grinding with silicon carbide papers from 320 to 2500 grit, and polishing to a final finish of 0.5 μm. The samples are etched with 4% Nital to reveal microstructural features. The microstructural characterization was performed using optical microscopy and scanning electron microscopy (SEM). Energy-dispersive X-ray spectroscopy (EDS) was used to analyze the elemental distribution. Furthermore, phase identification was carried out by X-ray diffraction (XRD) employing Cu Kα radiation ($\lambda = 0.154$ nm), with a scan step size of 0.0525° and a 2θ range from 10° to 140°. The surface hardness was measured using Vickers microhardness testing in accordance with ASTM E384. Indentations were taken across both surface and cross-sectional regions to evaluate hardness gradients and the integrity of the coatings.

Raman spectra were obtained with a Horiba Jobin Yvon LabRAM HR800 Raman spectrometer coupled to an Olympus BXFM optical microscope. The measurements were performed using a 632 nm laser excitation line, a 100× objective lens, and a 600 grooves/mm grating with a spectral resolution of 2 $cm^{-1}$/pixel. A multi-channel CCD detector was used, with integration times between 20 and 35 s. The spectra presented are without baseline correction.

Tribocorrosion behavior was evaluated using a pin-on-disk tribometer integrated with an electrochemical cell. These tests were performed in three different electrolytes: 0.1 M NaCl (pH 7), 0.001 M NaOH (pH 11), and sodium tetraborate (pH 10). An alumina ($Al_2O_3$) ball with a diameter of 6 mm used as the counterpart material. A ceramic $Al_2O_3$ ball was selected as the counterbody to ensure electrochemical isolation of the coated steel surface. The tribocorrosion procedure included a 30-min static immersion to stabilize the open circuit potential (OCP), followed by 1 h and 6 min of sliding under a normal load of 10 N at a sliding speed of 5 mm/s over a 10 mm track length, giving a total sliding distance of 20 m. A total sliding distance of 20 m was selected based on the preliminary tests that showed both the OCP and COF stabilized within the first 10–15 m, indicative of active tribocorrosion mechanisms. The estimated initial contact pressures were 1.6 GPa for the uncoated steel, 1.9 GPa for the borided surface, and 2.3 GPa for the NbC-coated specimen. A final 30-min static period was used to monitor electrochemical recovery after sliding. OCP was continuously monitored using a three-electrode configuration, with the sample as the working electrode, a platinum counter electrode, and an Ag/AgCl reference electrode. OCP monitoring was selected because it provides a sensitive, real-time indication of passive-film breakdown and repassivation during sliding. Although OCP does not quantify corrosion kinetics, the characteristic potential decrease and recovery trends offer direct insight into coating stability under mechanical-electrochemical interaction, which aligns with the mechanistic focus of this study. Additionally, dry sliding wear tests were also conducted under the same mechanical conditions (6 mm $Al_2O_3$ ball, 10 N load, 5 mm/s sliding speed, 10 mm track length, and 1 h 6 min duration) as a qualitative reference to establish the upper limit of purely mechanical damage in the absence of electrochemical effects, acknowledging that this condition does not replicate the lubrication or thermal behavior present during tribocorrosion. After the reciprocating sliding tests, wear volumes were assessed using the 3D confocal microscope, model Alicona Infinite Focus, from Alicona, Austria. The wear scars were further examined using a scanning electron microscope (SEM-EDS) to identify any wear-related failure mechanisms. To ensure sufficient reliability for the mechanistic comparisons, at least two parallel tests were conducted for all combinations, and the reported values represent the average of these independent measurements.

**Table 1**
The measured composition (in wt.%) of Vanadis 6 cold work tool steel.

| in wt.% | C | Si | Mn | Cr | V | Mo | Ni | Fe |
|---|---|---|---|---|---|---|---|---|
| V6 | 1.981 | 1.051 | 0.425 | 6.824 | 5.023 | 1.473 | 0.140 | Bal. |

## 3. Results and discussion

### 3.1. Microstructural characterization

Fig. 1 illustrates the microstructural characteristics of uncoated V6 tool steel following the conventional treatment. As shown in Fig. 1a, the microstructure is primarily composed of tempered martensite, accompanied by undissolved carbides of various sizes that are evenly distributed throughout the matrix. The backscattered electron image (Fig. 1b) and the corresponding energy-dispersive spectroscopy (EDS) micrograph provide further insight, enabling the identification of several carbide types: MC-type eutectic carbides enriched in vanadium, $M_7C_3$-type secondary carbides enriched in chromium, and $M_3C$-type alloyed cementite, which appears as small globular carbides (SGCs) [3]. Furthermore, X-ray diffraction analysis in Fig. 1c confirms the presence of these major phases in the V6 tool steel.

Fig. 2 presents scanning electron microscopy (SEM) cross-sectional images of V6 tool steel subjected to TCD treatments, specifically boriding and NbC coating. In Fig. 2, the borided sample displays a distinct dual-layer boride structure, consisting of an outer FeB layer and an inner $Fe_2B$ layer [19,36]. The measured total coating thickness ranges from 90

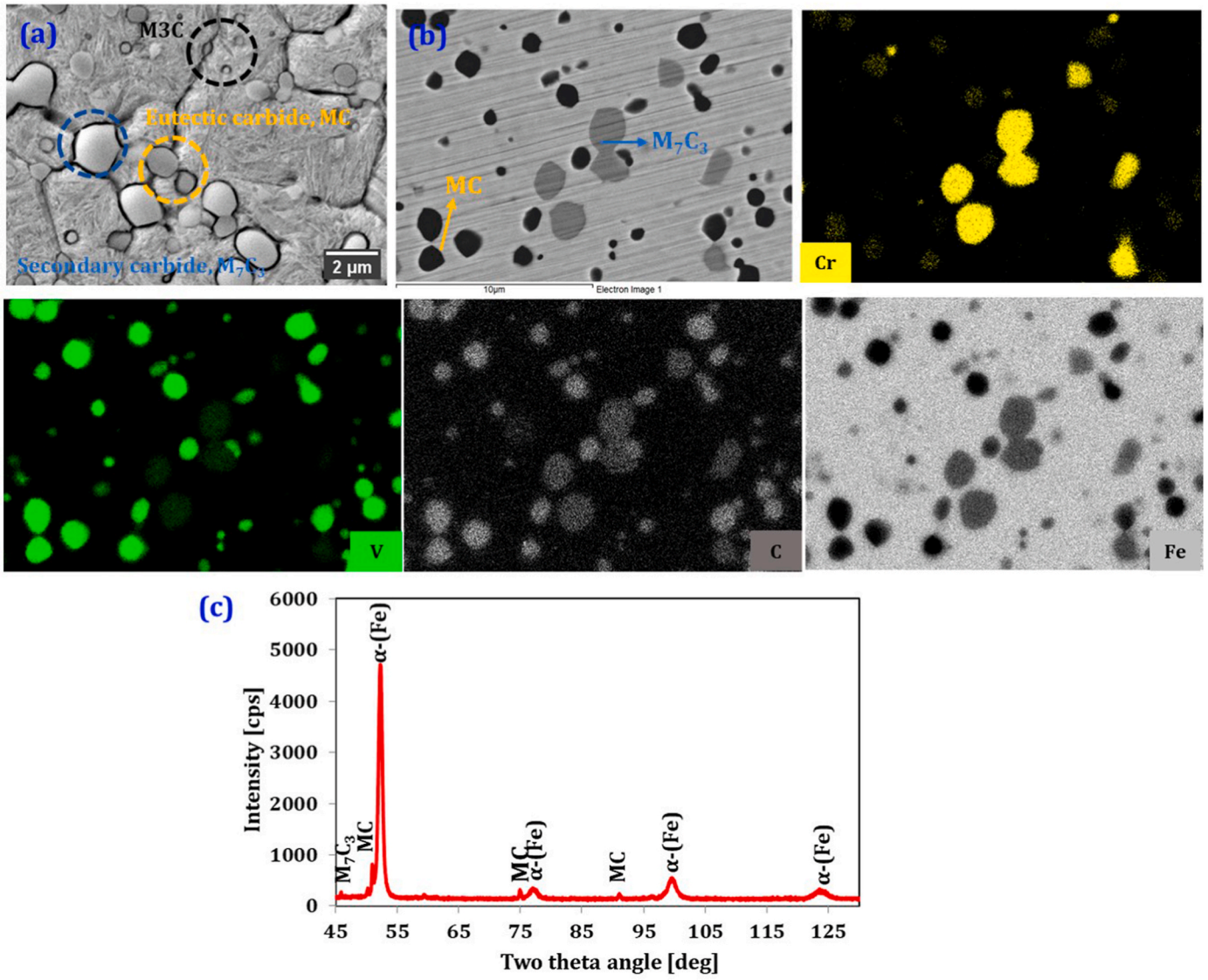


**Fig. 1.** SEM images showing microstructure of Vanadis 6 steel: (a). secondary electron image; (b). back scattered image and corresponding EDS maps of Chromium, Vanadium, Carbon, and Iron; and (c) X-ray diffraction phase analysis.

to 100 µm. From the SEM images it is observed that the FeB layer exhibits a compact planar morphology, while the $Fe_2B$ layer demonstrates a columnar growth pattern, which is the characteristic of diffusion-controlled kinetics. From the EDS maps it follows that insoluble chromium and vanadium carbides are embedded in boride layers.

In contrast, the NbC-coated samples (Fig. 3) exhibit a dense, smooth, and single phase structure [6,20]. The coating thickness is between 10 and 15 µm, and there is negligible diffusion of niobium into the substrate. As a result, no concentration gradient of niobium is observed at the interface between the coating and the substrate. Furthermore, EDS mapping as shown in Fig. 3, confirms the elemental composition of the coating region and indicates the formation of a niobium-rich phase.

X-ray diffraction (XRD) analysis as presented in Fig. 4 further supports these microstructural observations. In the borided sample (3B), FeB is the dominant phase with the presence of $Fe_2B$ phase (Fig. 4a). For the NbC coated surfaces, the primary diffraction peaks correspond to the NbC phase (Fig. 4b), with martensite identified as a secondary phase from the substrate.

### 3.2. Hardness

Microhardness measurements were conducted on the cross-sectional surfaces of both borided (B), and niobium carbide (NbC) coatings, and the polished uncoated surface. Multiple indentations were performed on the polished surfaces, and the average values are reported. Additional data on coating thickness and surface roughness, along with microhardness values, are summarized in Table 2.

The uncoated substrate exhibited a hardness of 710 HV30, reflecting the tempered martensite matrix. After boriding, the surface hardness increased significantly to approximately 2000 HV0.1. This notable increase in hardness is consistent with the formation of FeB and $Fe_2B$ phases, which are known for their high hardness. The NbC coated samples also demonstrated a considerable increase in hardness, with the mean value of 1550 HV0.1. Although this value is lower than that of the borided specimen, the NbC coating exhibited a more uniform hardness distribution across the coating thickness. The hardness values obtained in this study align within the previously reported ranges for borided steels. For instance, Yapici et al. [40] reported hardness values between 2005 and 2227 HV0.1 for borided AISI D2 steel processed under comparable thermochemical conditions. Similarly, Resendiz-Calderon et al.

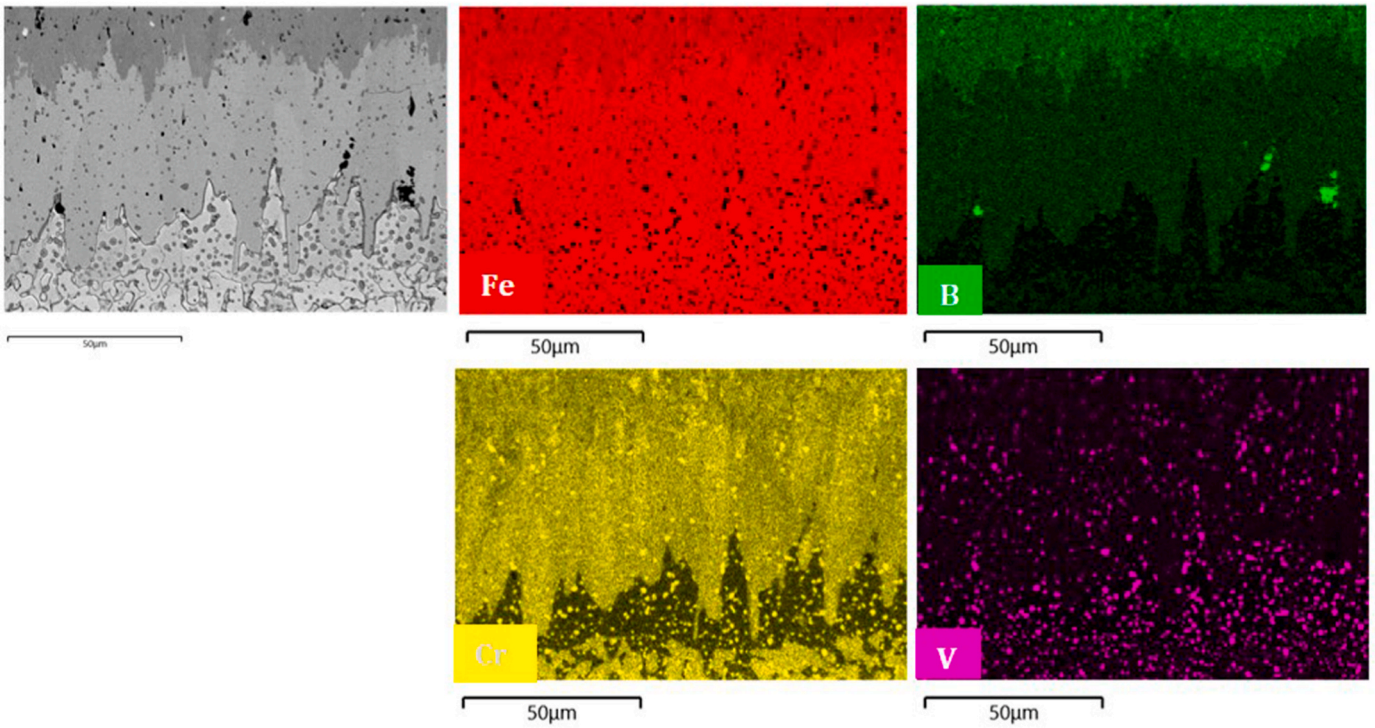


**Fig. 2.** Cross-sectional SEM microstructure of borided V6 tool steel with corresponding EDS maps.

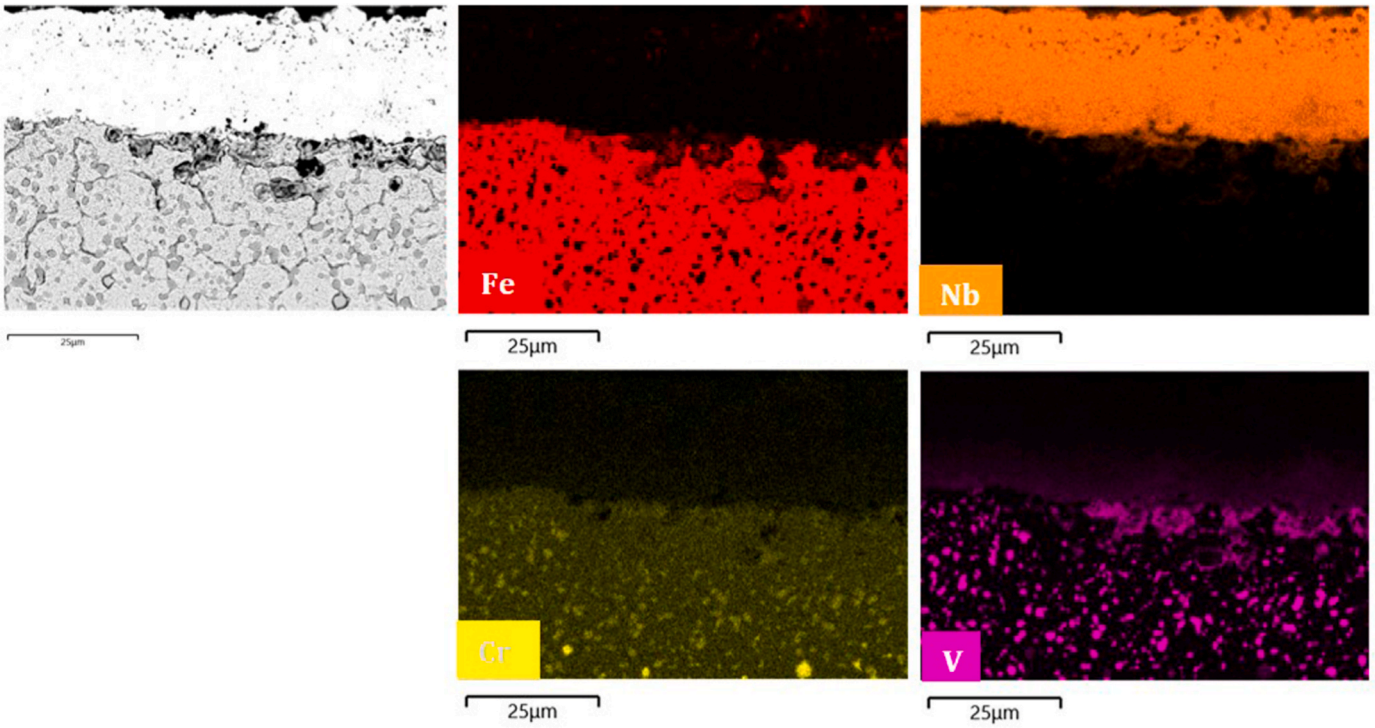


**Fig. 3.** Cross-sectional SEM microstructure of NbC-coated V6 tool steel with corresponding EDS maps showing no diffusion of Nb into the substrate.

[41] reported a mean hardness of 2007 HV0.03 for borided D2 steel. In the case of NbC coating, Castillejo et al. [42] demonstrated that the incorporation of Nb-rich carbides can elevate the surface hardness to approximately 2166 HV in D2 steel, while Mariani et al. [43] reported values in the range of 2332 and 2345 HV0.5 for ductile cast iron subjected to NbC coating. Although the hardness values measured in the present work are somewhat lower than those reported in the literature, these differences can be attributed to variations in alloy composition, diffusion kinetics, and processing parameters such as temperature, duration, and activation chemistry.

Overall, the hardness results obtained in this study demonstrate the effectiveness of both thermochemical diffusion treatments in improving the surface mechanical properties of V6 tool steel. Among the two processes, boriding produced the highest hardness levels, consistent

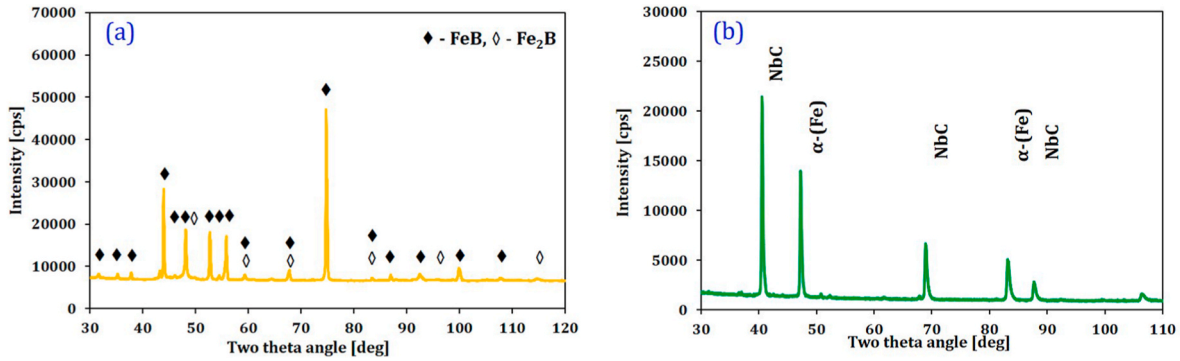


**Fig. 4.** Xray diffraction analysis of differently coated V6 tool steel: (a). Borided; (b). NbC coated.

**Table 2**
The coating thickness, microhardness, and surface roughness of V6 cold work tool steel.

| Treatment | Coating Thickness (μm) | Surface Roughness, Ra (μm) | Microhardness (HV) |
|---|---|---|---|
| Uncoated | 0 | 0.75 ± 0.20 | 710 ± 32 HV30 |
| Boriding | 90-100 | 0.39 ± 0.03 | 2000 ± 119 HV0.1 |
| NbC-coating | 10-15 | 0.92 ± 0.66 | 1550 ± 97 HV0.1 |

with the formation of hard boride phases.

### 3.3. Friction and mechanical wear

The coefficient of friction (COF) as a function of sliding distance for the uncoated and coated specimens along with the average COF values are shown in Fig. 5. The presented results refer to the dry sliding condition. Although the interfacial conditions differ from those in an electrolyte, the dry sliding is used as a control condition to represent the upper limit of purely mechanical wear. From the graphs, it is noticed that the COF response of the uncoated, borided, and NbC-coated steels shows clear differences in both the running-in period and the steady-state regime. These trends correlate strongly with the initial surface roughness, contact pressure, and coating mechanical properties.

For example, the uncoated sample maintained the highest COF throughout the test, with a mean value of 0.58 and the most pronounced running-in state. Its moderate surface roughness (Ra ≈0.75 μm), lowest initial contact pressure (1.6 GPa) combined with the low hardness promotes plastic deformation, micro-cutting, and ploughing, which are the characteristic of adhesive and abrasive wear interactions. Similar high and unstable COF values have been reported for uncoated cold-work and hot-work tool steels sliding against $Al_2O_3$ counterparts, where severe plastic deformation and ploughing govern the tribological response [40,44]. In contrast, the borided surface shows a substantially lower COF response (0.48) and running-in period similar like uncoated sample. The lower roughness (Ra ≈0.39 μm) and higher hardness reduce the real area of contact and suppress plastic deformation, resulting a stable and lower COF value. However, after a short running-in period, the COF curve showed more fluctuations suggesting the local disruptions caused by micro-fracture of the coating due to brittleness. The NbC coated sample also showed a mean COF value of 0.48, but its sliding curve was more stable than that of the borided and uncoated sample. Despite having the highest roughness (Ra ≈0.92 μm) and initial contact pressure (2.3 GPa), the NbC layer does not show an extended or pronounced running-in stage. Instead, the COF curve indicates a smooth transition to steady-state. This suggests that the early asperity interactions or limited micro-fracture do not significantly disturb the COF response. This behavior may be attributed to the high surface hardness and chemical stability of NbC-based diffusion layers.

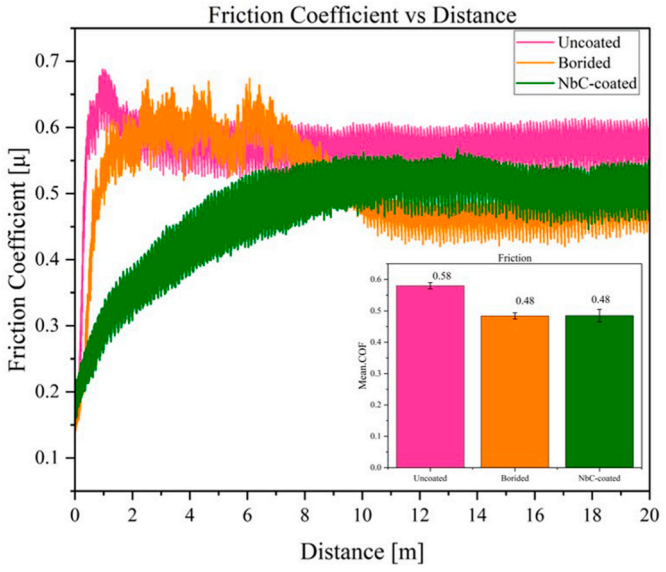


**Fig. 5.** Coefficient of friction values as a function of sliding distance for uncoated and differently coated V6 samples.

Overall, the coatings achieved a 17.24% reduction in friction relative to the uncoated sample, demonstrating a clear improvement in tribological performance. This reduction is consistent with the increased hardness of both coatings, which limits adhesion and mitigates the severity of asperity interactions. Lower friction associated with hard coatings has been widely reported in the literature, and the present results follow this established trend. Yapici et al. [40] borided AISI D2 steel at 900 and 1000 °C for 3, 5, and 7h and evaluated its sliding behavior against an $Al_2O_3$ ball under loads of 10, 20, and 30 N. They observed that the COF of the borided layer produced at 1000 °C stabilized in the range of 0.5-0.6, compared with 0.6-0.7 for the uncoated steel. Similarly, Castillejo et al. [42] deposited NbC, chromium carbide, and mixed niobium-chromium carbide coatings on AISI D2 steel using the TCD process. Under the 4 N load against $Al_2O_3$ ball, the coated samples exhibited COF values between 0.25 and 0.32, whereas the uncoated sample showed values 0.6-0.7, further confirming the friction-reducing capability of carbide-based diffusion coatings. Collectively, the literature indicates that both borided layers and NbC coatings consistently yield lower friction coefficients than uncoated specimens across multiple alloy systems [6,41,43,45]. These findings highlight the critical role of coating selection in applications requiring consistent low-friction behavior, particularly under dry sliding conditions where abrasive and adhesive wear mechanisms dominate.

Furthermore, the measured wear volumes as in Fig. 6 show a clear dependence on the hardness differences between the samples and the alumina counter-body. The estimated microhardness of the sintered

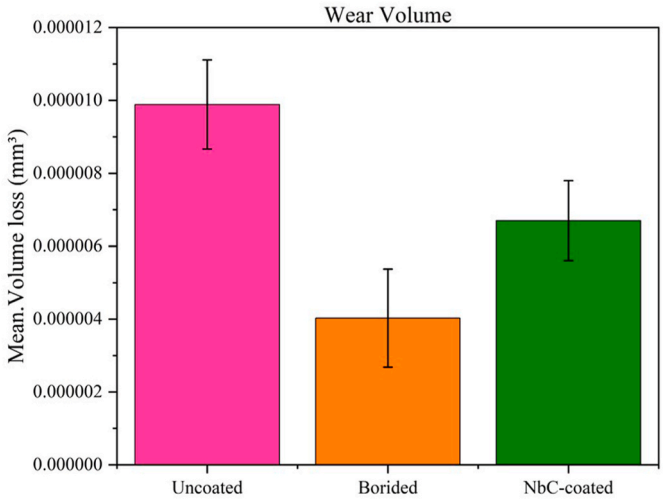


**Fig. 6.** Mean wear volume loss ($mm^3$) of uncoated and differently coated V6 samples after dry sliding wear tests.

alumina ball is approximately 1450-1600 HV [46]. So, the uncoated steel, with a hardness of 710 HV, exhibits the highest wear volume (~$9.89 \times 10^{-6}$ $mm^3$). This material loss is consistent with the substantial hardness gap relative to the alumina ball, which promotes severe micro-cutting and ploughing during the sliding. This suggests that the soft substrate is unable to resist asperity penetration, leading to accelerated material removal. In contrast, the borided specimen, with a surface hardness of 2000 HV, shows the lowest wear volume (~$4.02 \times 10^{-6}$ $mm^3$). The FeB and $Fe_2B$ layers are significantly harder than the uncoated specimen, enabling the coating to resist penetration and plastic deformation. This hardness advantage reduces the severity of abrasive interactions and limits the depth of micro-cutting. The reduced wear volume indicates that the boride layers provide an effective load-bearing capacity despite the presence of cracks and micro pits observed in the wear tracks due to the low fracture toughness of borides. For instance, Orihel et al. [47] studied the fracture toughness of boride layers on tool steels using Palmquist indentation method. They reported that the mean fracture toughness of FeB and $Fe_2B$ layers was 1.98 and 4.5 MPa $m^{1/2}$, respectively. In a similar study, Ucisik et al. [48] studied the crack propagation and fracture toughness of FeB/$Fe_2B$ layers on low-alloy steels. They found that the fracture toughness of the borides ranged from 4 to 6 MPa $m^{1/2}$. However, it should be noted that the reported variations in the fracture toughness mainly depend on the chemical composition of the substrate and the boriding time.

On the other hand, the NbC-coated specimen, with a hardness of 1550 HV, exhibits an intermediate wear volume (~$6.70 \times 10^{-6}$ $mm^3$). Although harder than the uncoated steel, its hardness is lower than that of the borided surface, thereby reducing the effective wear-protection margin. The NbC layer provides substantial resistance to plastic deformation; however, its performance is constrained by its intrinsically low fracture toughness (~1.15 MPa $m^{1/2}$) [45], which promotes brittle micro-fracture under sliding contact. This brittleness likely contributes to the formation of micro-pits and localized material pull-out, explaining the slightly higher wear loss relative to the borided specimen. Zhao et al. [49] performed a detailed scratch-test study on NbC coatings and reported that crack density increased progressively with applied load. Their topographical analysis confirmed that NbC coatings exhibited a brittle fracture response despite maintaining acceptable adhesion to the substrate. Such observations are consistent with the wear behavior observed in the present study. The enhanced wear resistance of tool steels treated via boriding and NbC coating has been widely attributed to the substantial hardness increase imparted by these diffusion-based surface layers [6,41,43,45]. The results obtained in the present study corroborate these findings and highlight the critical role of hard diffusion coatings in demanding tribological applications.

Besides, the observed SEM imaging of the wear tracks collaborates with the findings presented in the wear volumes. For instance, the uncoated surface shows severe micro-cutting, ploughing, and plastic deformation experiencing greater material loss. In contrast, both borided and NbC-coated surfaces showed no signs of plastic deformation rather showed extensive microcracks and pitting due to the lack of toughness [47,49] when compared to the uncoated surface. Comparable wear-track morphologies have been widely reported for hard-coated steels tested against $Al_2O_3$ counterparts. For example, Yapici et al. [40] examined borided AISI D2 steel under reciprocating sliding and observed micro-cracks, boride-layer fractures, and oxide-rich regions on the worn surfaces at a 10 N. Similarly, Da Costa Aichholz et al. [50] investigated the tribological and tribocorrosion performance of borided AISI 4140 steel against 6 mm $Al_2O_3$ ball and reported abrasive wear, plowing, and oxide formation on the uncoated specimen, whereas the borided samples exhibited finer, shallower abrasive grooves and discrete pit formation. The detailed SEM micrographs illustrating these wear-track morphologies and associated damage mechanisms are provided in Fig. 7.

Additionally, the SEM examination of the wear tracks showed dark patches distributed along the sliding path on all samples. To clarify their origin, EDS mapping was performed on all the specimens, and the corresponding elemental distributions are shown in Fig. 8.

The maps indicate that these dark regions contain elevated levels of oxygen and presence of aluminum, suggesting that they consist of alumina-rich oxide films formed during sliding. Their presence across all samples suggests that oxidative wear is a common mechanism regardless of coating type. Importantly, the dark-patch regions on the coated samples did not show boron or niobium carbide signals, indicating that the oxide layer forms from the exposed regions where coating fractured. This absence suggests the local cracking and micro pitting, enabling brittle micro-fracture and delamination of the coating layer causing oxidative wear debris. On repeated sliding the oxidative wear debris may act as three-body abrasive particles further accelerating the material loss [50]. The presence of aluminum confirms the material transfer from the $Al_2O_3$ counter-body. This transfer is consistent with the hardness interactions where the coating hardness exceeds that of the ball ranged from 1450 to 1600 HV, the counter-body undergoes micro-fracture or material removal. Together, these observations indicate that the dark patches represent alumina-oxide tribofilms, which developed through a combination of counter-body transfer and subsequent oxidative modification.

### 3.4. Tribocorrosion performance

The tribocorrosion tests were performed in three electrolytes−0.1 M NaCl (pH 7), 0.001 M NaOH (pH 11), and Na-tetraborate (pH 10) −using the same test parameters as in the dry wear tests. The open circuit potential (OCP) was monitored throughout a three-stage protocol comprising a 30-min static immersion, a 1 h and 6-min sliding phase, and a final 30-min static recovery period. This approach enabled simultaneous evaluation of electrochemical and tribological responses under dynamic conditions.

Fig. 9 presents the potential measurements at open circuit potential for three different samples: uncoated (3), borided (3B), and NbC-coated (3N) in NaCl solution. The OCP values change when metal is initially exposed to the electrolyte. The direction of potential value change shows protective behavior of metals when OCP value increases, or, OCP value decreases when porous hydroxide layer or corrosion products are formed [51].

During initial immersion up to approx. 2000s, the OCP potential decreased and reached a quasi-steady state. The OCP potential was more negative of uncoated, −0.57 V and borided sample (−0.52 V). The NbC coated sample had potential more positive, at −0.31 V. During the start of rubbing, OCP potential stayed similar for uncoated sample, only for

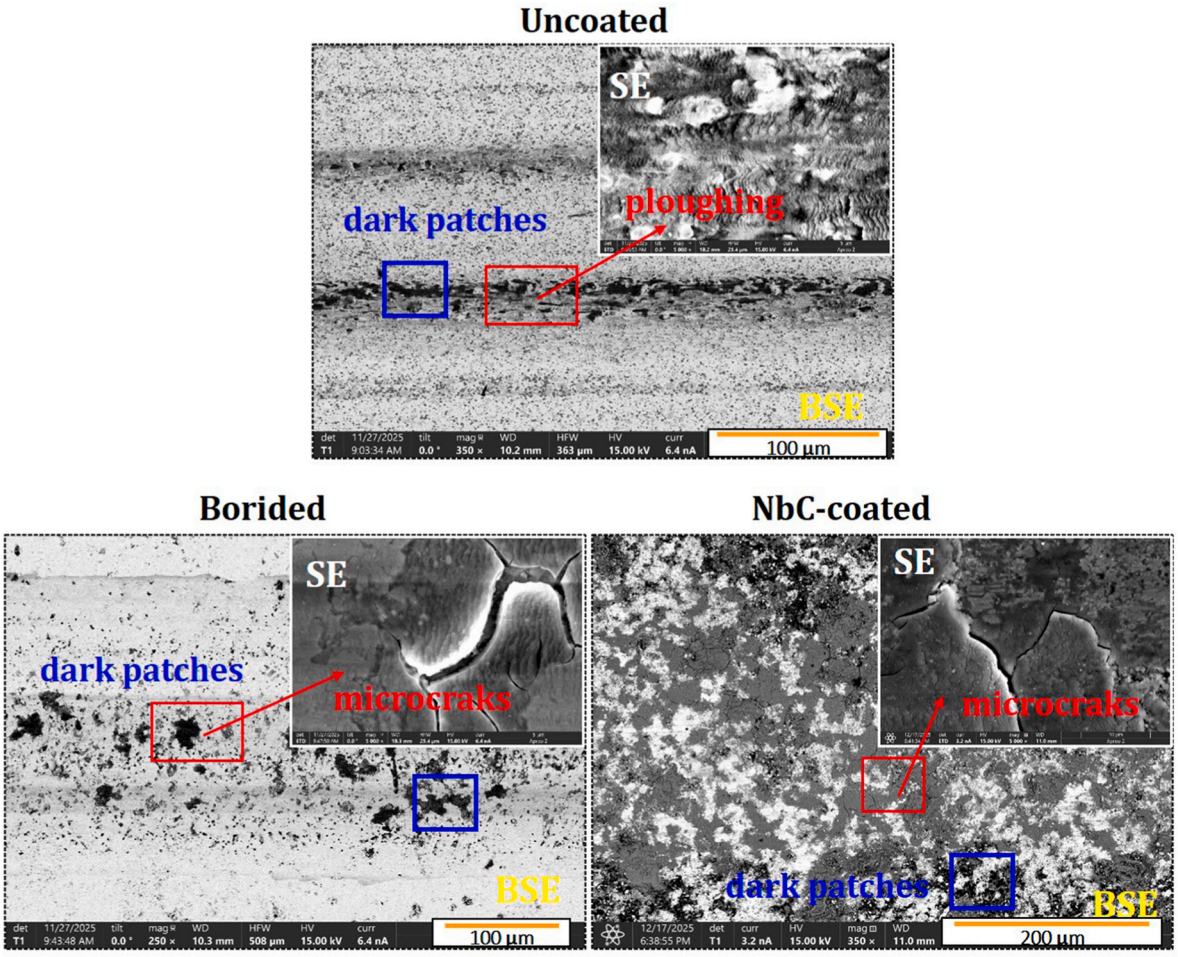


**Fig. 7.** Wear track morphology of uncoated and differently coated V6 samples after dry sliding wear tests with corresponding back scattered electron (BSE) and high magnification secondary electron (SE) images.

NbC coated sample it decreased to a value around −0.39 V. In the borided sample, the potential increased with the onset of wear. This is because the electrolyte reaches the base metal during the wear process. The wear zone acts as the anode and the non-wear zone as the cathode in steels with a protective layer, such as stainless steels, due to mechanical damage; while the opposite behavior occurs in carbon steels [23].

After the end of rubbing, the uncoated sample exhibited similar values at −0.55 V vs. Ag/AgCl, although the potential was not recorded. The uncoated sample actively corroded in 0.1 M NaCl, as expected. The borided sample showed slightly lower potential values at −0.54 V. On the other hand, the NbC-coated sample exhibited no potential change after the end of rubbing, but potential values slowly decreasing to a value −0.43 V at the end of tribocorrosion test. The more positive OCP values indicate the superior barrier properties of the NbC layer. The OCP remained stable during sliding, with no significant difference between rubbing and non-rubbing conditions. Although the 3N sample showed the best performance, its potential decreased toward the end of the abrasion process, likely due to the limited thickness of the NbC coating.

In contrast, both coated samples demonstrated more noble potentials throughout the test, suggesting enhanced corrosion resistance. The borided sample showed intermediate performance, with potential values ranging from −0.51 V and −0.53 V. On the other hand, the NbC-coated sample exhibited passive surface characteristics, maintaining potentials at −0.39 V during rubbing. After the end of rubbing, the potential did not recover for NbC-coated sample. The stability of the OCP during sliding for NbC-coated sample further suggests that the coating resists mechanical disruption and maintains its protective function under tribological stress.

The OCP results in 0.001 M NaOH solution are presented in Fig. 10. Unlike the behavior observed in NaCl, the alkaline environment resulted in a different ranking of corrosion resistance among the samples. The borided sample exhibited the most negative and less stable potential throughout the test. It initiated at appropriately −0.45 V and declined further to around −0.5 V with observed fluctuations during sliding, with further decrease in potential in the final phase. This behavior suggests poor passivation and high susceptibility to hydroxide-induced degradation. The boride layer, which may offer protection in chloride environments, appears less effective in alkaline conditions-possibly due to partial dissolution or instability of boride phases at elevated pH.

Noticeably, the uncoated sample demonstrated intermediate electrochemical performance. It began at −0.41 V and stabilized near −0.43 V, with moderate fluctuations during sliding. After the end of rubbing, a slight increase in potential is observed. The relatively more positive potential compared to 3B indicates slightly improved resistance to corrosion, likely due to the formation of iron hydroxide surface films (confirmed by Raman analysis, Fig. 14) that offer temporary passivation. The NbC-coated sample exhibited the most positive OCP potential during the tribocorrosion test. Its initial OCP value decreased from −0.04 V to −0.19 V at the onset of rubbing. Upon sliding, the potential of 3N sample decreased and then remained low and nearly stable throughout the wear period. Although no abrupt increase was observed after the end of wear, a gradual recovery of the potential occurred, indicating passive behavior of the coating. The limited variation during sliding and the moderate recovery in the final phase reflect the robustness of the NbC

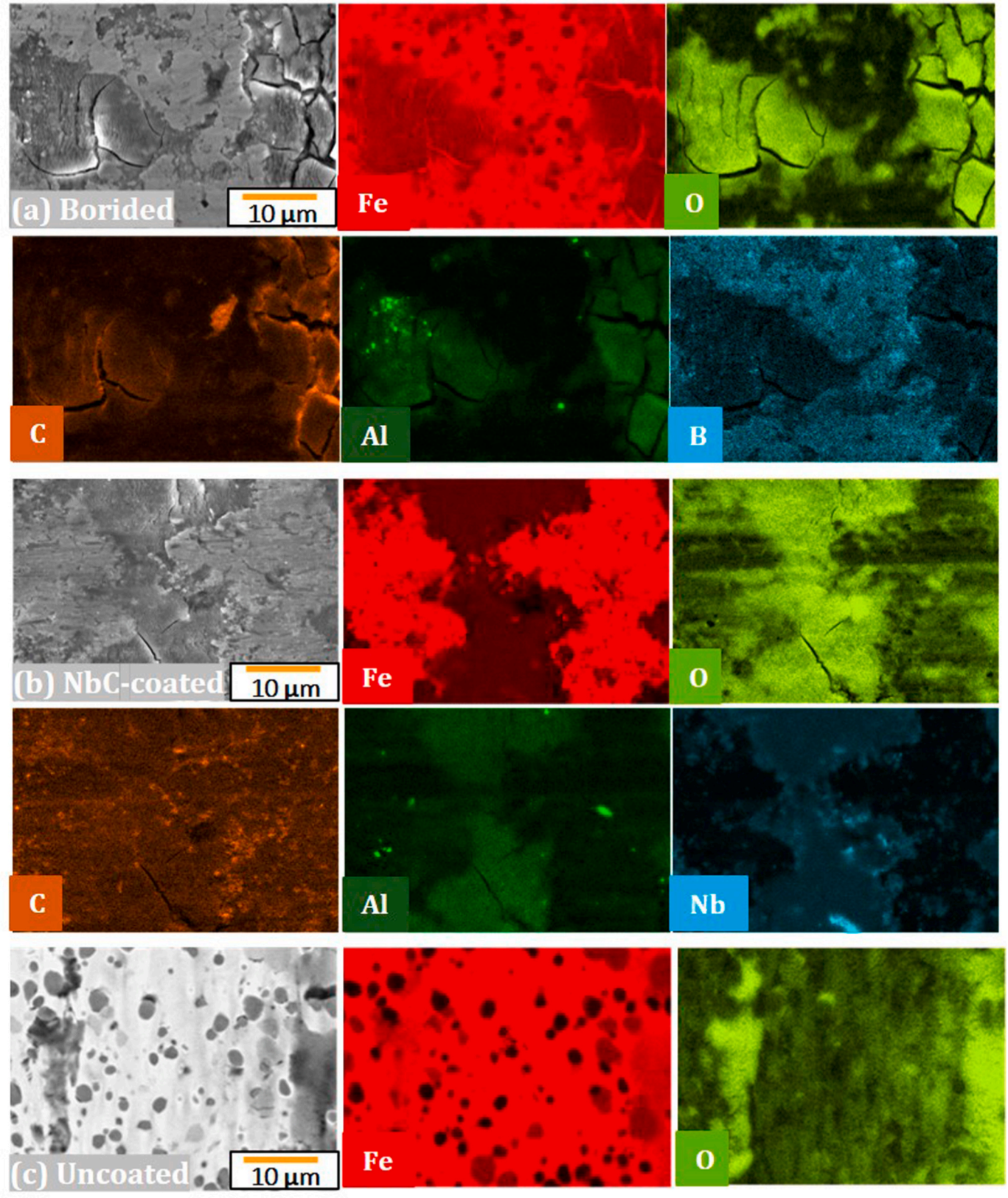


**Fig. 8.** EDS elemental mapping of wear track for borided, NbC-coated, and uncoated V6 sample after dry sliding test showing dark-oxide patches.

layer in alkaline media.

Furthermore, the OCP results in Na-tetraborate solution with pH 10 showed distinct trends as shown in Fig. 11. The borate solution induced different behavior when studying tribocorrosion properties of the samples in comparison with the behavior noticed in NaCl and NaOH. The NbC-coated sample maintained the most noble potential response throughout the testing. During initial immersion the potential for both coated samples decreased slightly with time and showed similar values

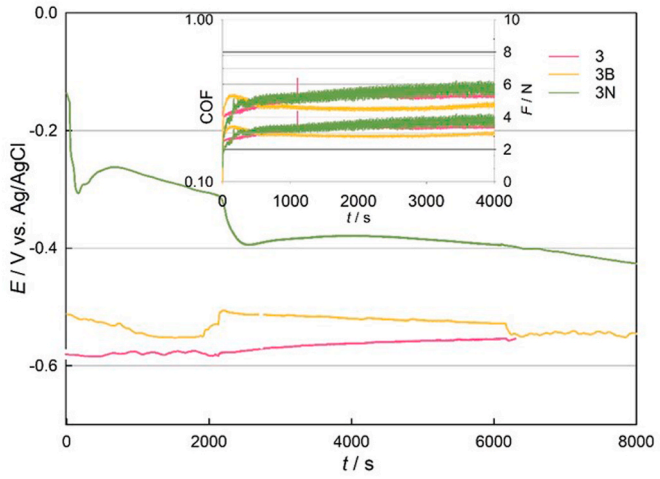


**Fig. 9.** Open circuit potential of uncoated and differently coated V6 tool steel in NaCl solution.

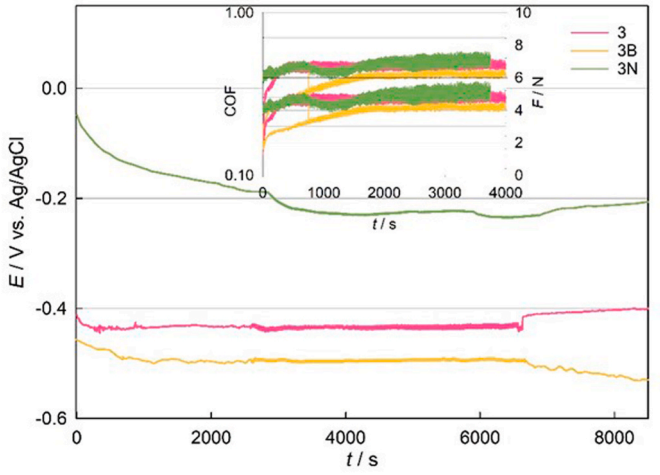


**Fig. 10.** Open circuit potential of uncoated and differently coated V6 tool steel in NaOH solution.

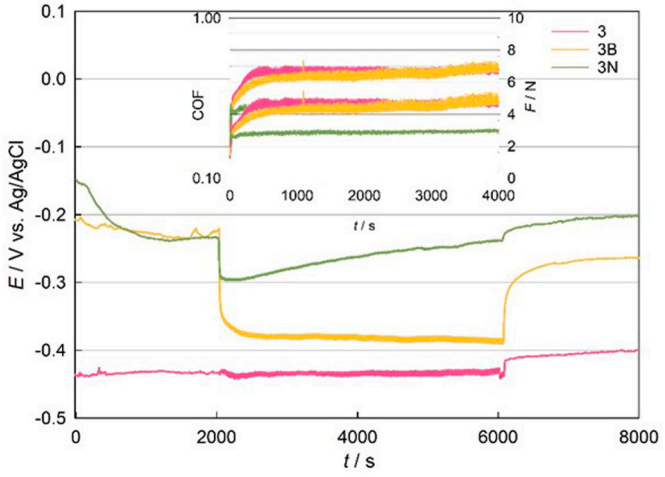


**Fig. 11.** Open circuit potential of uncoated and differently coated V6 tool steel in Na-tetraborate buffer solution.

at −0.23 V just before rubbing, while OCP value for uncoated sample stayed at stable value of −0.43 V. During sliding, the potential of coated samples decreased to a value of −0.38 V for 3B sample and −0.29 V for 3N sample.

For 3N sample, the potential shifted toward positive values during sliding, indicating that the tribological contact did not compromise passivation but instead promoted a more protective interfacial state. The post sliding recovery sustained this nobility, reflecting a chemically inert and mechanically resilient. The borided sample ranked second in nobility. Its OCP remained nearly constant during sliding-more stable, but did not exhibit the positive excursion seen for 3N. After the end of sliding, the potential rapidly moved toward more positive values, evidencing swift repassivation once mechanical disruption ceased. This behavior suggests that the boron-derived surface film is sufficiently protective in static borate exposure but less capable than NbC of enhancing passivation under active tribological contact; instead, it recovers rapidly when the mechanical stimulus is removed. The uncoated sample was the least noble across the test, with OCP remaining below −0.43 V during immersion and holding nearly constant through the sliding interval. Only in the recovery phase the potential increased slightly, reaching approximately −0.40 V, indicating repassivation in the absence of mechanical abrasion.

Although chloride-containing solutions such as NaCl are widely employed to simulate aggressive service environments, their high corrosivity can hinder the tribological contribution to degradation, particularly alloys like tool steels that are not inherently passive. In contrast, Na-tetraborate buffer (pH-10) provides a less aggressive conductive medium that allows distinct differentiation of tribocorrosion behavior under sliding conditions. The OCP profiles obtained in Na-tetraborate buffer reveal that both coated samples (NbC and borides) begin with similar potentials, but their responses diverge during sliding: the NbC-coated steel shifts toward more positive values, indicating enhanced passivation under tribological stress, while the borided steel remains nearly constant before rapidly moving noble in the recovery phase. The uncoated steel, by comparison, remains at more negative potentials during sliding and recovery without a strong repassivation capability. This behavior highlights the interplay between mechanical film disruption and electrochemical recovery, which is more readily observed in borate environment than in chloride or strong alkaline solutions. Thus, Na-tetraborate buffer offers a balanced test medium: sufficiently corrosive to reveal differences in coating performance, yet mild enough to prevent dissolution and masking tribological effects. For tool steels, which lack strong intrinsic passivation, this electrolyte provides a controlled environment to evaluate surface modifications influencing tribocorrosion resistance. The ability to capture both sliding-induced potential shifts and post-sliding recovery makes Na-tetraborate buffer suitable for comparative studies, ensuring that the protective mechanisms of coatings are assessed under conditions where tribological factors are not hindered by corrosion of steel.

### 3.5. *Surface analysis of post-tribocorrosion*

SEM observations of the wear tracks after tribocorrosion testing in NaOH and Na-tetraborate buffer are shown in Fig. 12. In this case, similar wear characteristics were found in the samples after testing in NaCl and NaOH; therefore, only a representative comparison with NaOH and Na-borate buffer has been presented.

The NbC-coated sample was notable for its responsiveness to solution chemistry. This represents a significant difference in tribocorrosion performance across the various solutions tested. For example, in NaOH, the wear track on the NbC exhibited wide abrasive grooves and microcracks (refer, Fig. 12), suggesting moderate material degradation resulting from corrosion-accelerated dissolution. This occurred because the protective tribofilm is thermodynamically unstable in a strong alkaline solution. This can be noticed from the OCP curve in Fig. 10 as varied potentials observed during sliding. In contrast, when tested in Na-tetraborate solution, the same sample demonstrates the strong

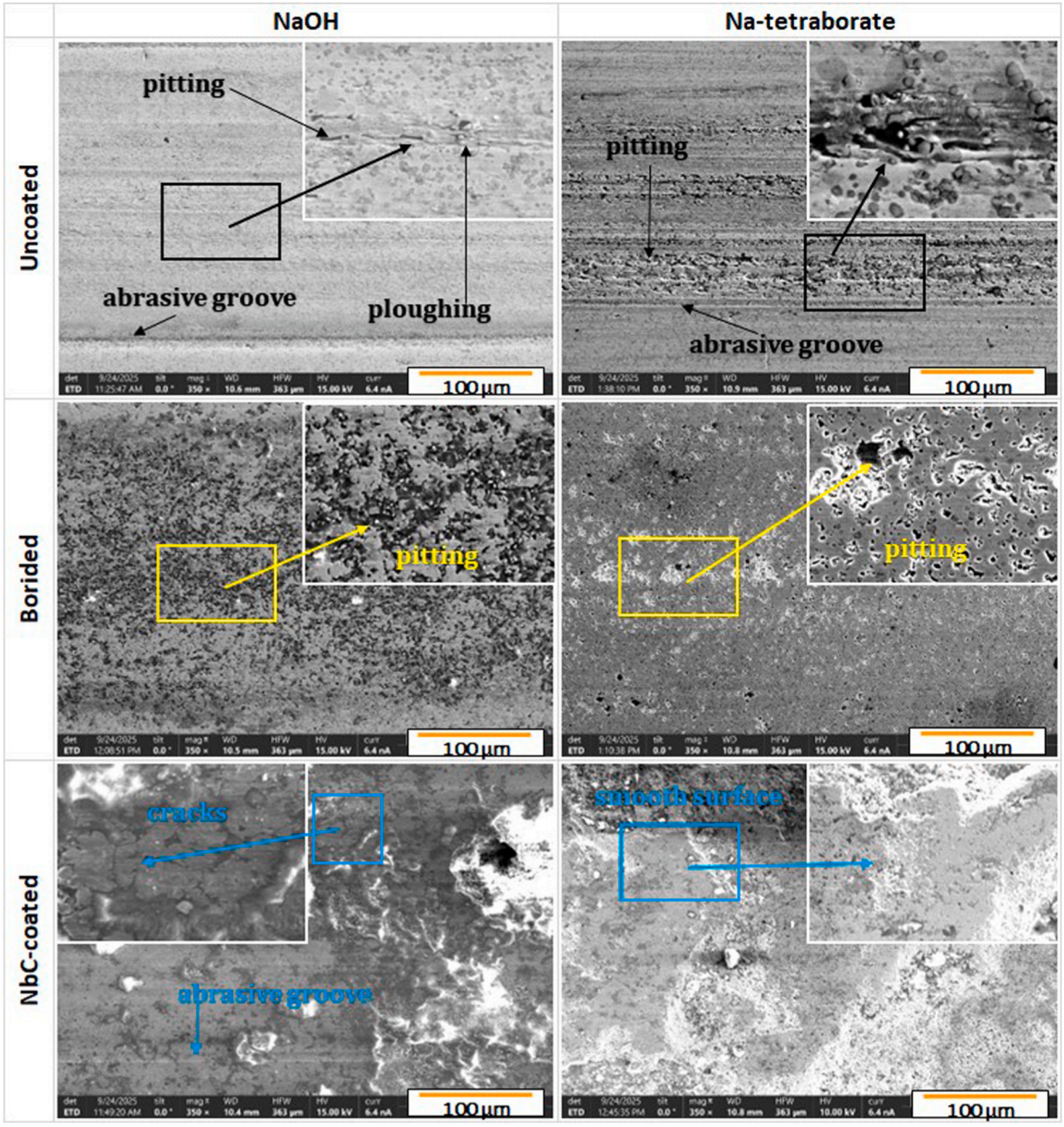


**Fig. 12.** SEM analysis of wear tracks that were tested in NaOH and Na-tetraborate buffer solutions.

repassivation of the protective tribofilm, as noticed in Fig. 11 with increased potential.

On the other hand, the borided sample demonstrated considerable pitting and material degradation in NaOH solution. However, the wear track in Na-tetraborate buffer solution revealed a smooth surface with no indications of severe pitting, yet occasional pits or cavities observed. This indicates, the exposed coating was swiftly attacked, resulting in wear-accelerated corrosion. In the case of borided sample in Na-tetraborate solution, this secondary corrosion was inhibited, thereby confirming the protective role of borate ions. The EDS maps of the wear tracks tested across all solutions following the tribocorrosion tests indicated oxidation damage and third-body abrasive wear mechanisms, as shown in Fig. 13. It is important to note that only the EDS maps from the NaCl solution are shown here, yet in all tested scenarios, the coatings provided substrate protection, as observed in the EDS maps.

When compared, the uncoated sample exhibited an extensive damage in all tested environments. Its wear was predominantly a result of two-body abrasion, resulting in parallel abrasive grooves indicative of ploughing and plastic deformation, accompanied with moderate pitting corrosion in NaOH and severe pitting corrosion in Na-tetraborate solution, refer Fig. 12. Overall, the results show clear differences in the failure mechanisms. The NbC-coatings performs best in solutions that support passive-film stability, followed by the borides. The uncoated sample shows the lowest resistance in most of the environments tested.

Furthermore, the corrosion products were identified using Raman spectra for all of the samples tested in Na-tetraborate solution. Analysis of the Raman spectra in Fig. 14 clearly revealed the existence of three different iron oxide corrosion products across different surface conditions. For both the uncoated and borided specimens, examination of the Raman spectra collected inside and outside the wear track confirmed the formation of magnetite ($Fe_3O_4$), characterized by its intense peak at 659 $cm^{-1}$, along with hematite ($\alpha$-$Fe_2O_3$), identified through its representative bands at 228, 286, 407, and 503 $cm^{-1}$. In contrast, the NbC-coated specimen exhibited the formation of goethite ($\alpha$-FeOOH), indicated by its most intense peaks at 311 and 390 $cm^{-1}$, accompanied by additional representative peaks at 488, 530, and 672 $cm^{-1}$ [52].

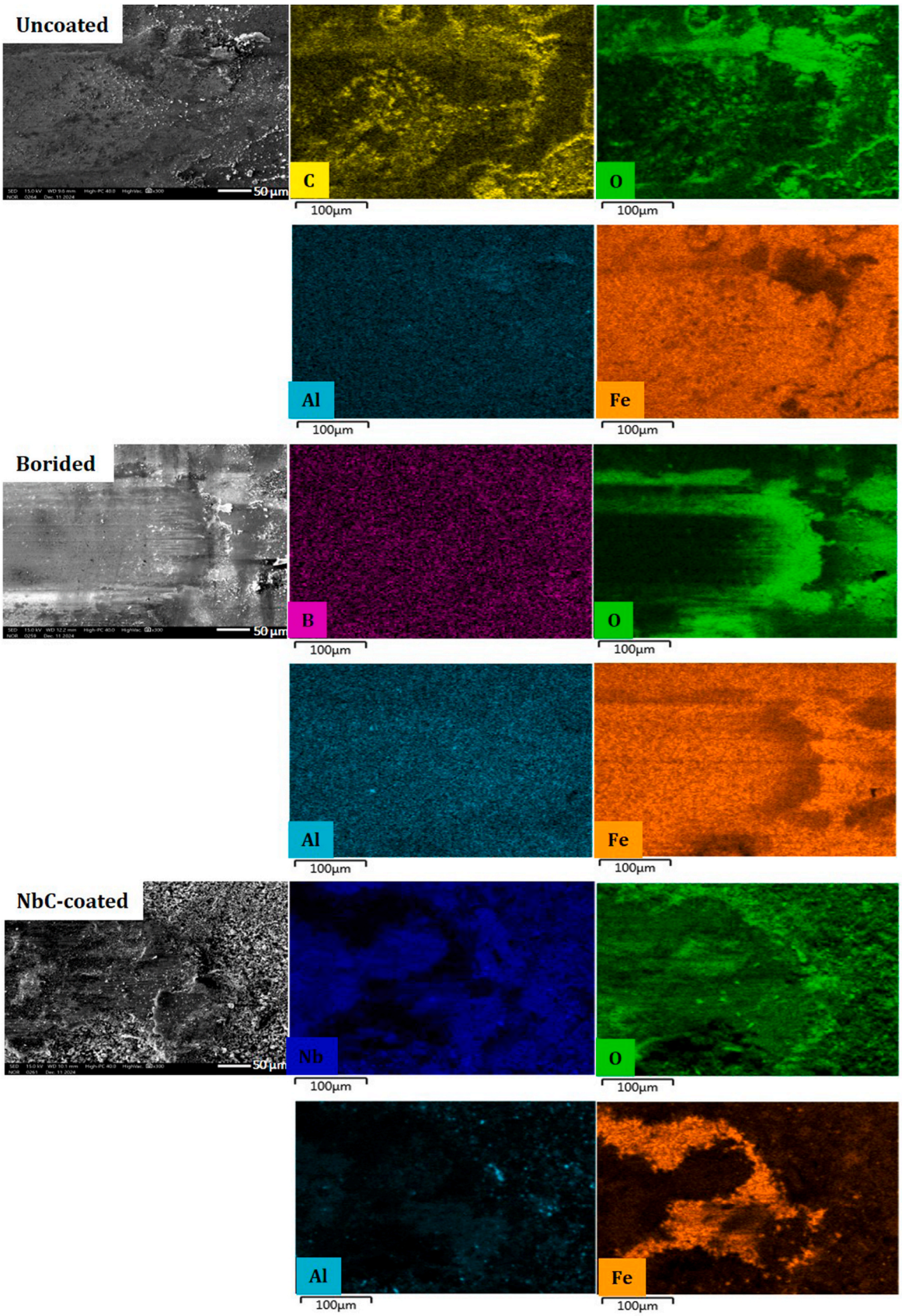


**Fig. 13.** SEM-EDS analysis of wear tracks after testing in NaCl showing enriched oxygen and iron in the wear tracks as dark patches.

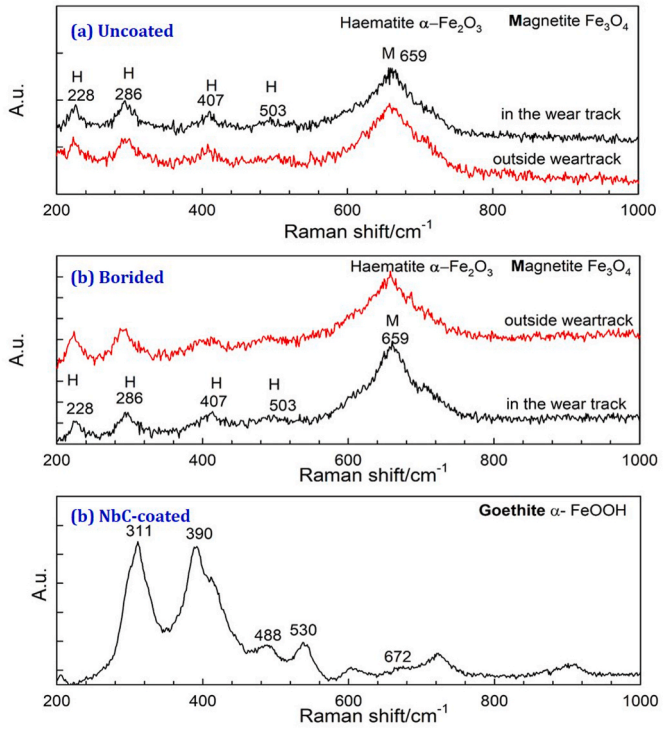


**Fig. 14.** Raman analysis of wear tracks after testing in Na-tetraborate solution showing different corrosion products.

The tribocorrosion behavior of the V6 steel can be interpreted by correlating the electrochemical response with the post-wear morphological and chemical analysis. The OCP signal exhibited a characteristic drop at the onset of sliding for all tested combinations, indicating rupture of the passive film due to mechanical action. The subsequent partial recovery of the potential during sliding interruptions reflects the repassivation tendency of the exposed surface. These depassivation-repassivation cycles are consistent with early-stage tribocorrosion behavior reported for hard coatings and several grade materials [21,24,25]. SEM and BSE imaging of the wear tracks revealed oxide-rich patches, smeared regions, and compacted debris both within and adjacent to the wear scars. These features are characteristics of tribo-oxidation. EDS mapping confirmed localized oxygen enrichment in these regions, indicating active oxidation during sliding and supporting the electrochemical activation inferred from the OCP response. Raman spectroscopy provided further chemical confirmation of the tribocorrosion mechanism, identifying oxide compounds formed in situ. The presence of these oxide phases aligns with the observed OCP fluctuations and the oxygen-rich debris detected by EDS. Taken together, the electrochemical response and post-wear analysis consistently indicate that the dominant degradation mechanism involves repeated cycles of passive-film rupture and repassivation, coupled with mechanically assisted oxide formation and removal.

The present study evaluates the tribocorrosion behavior of uncoated, borided, and NbC-coated Vanadis 6 steel, but several inherent limitations should be acknowledged. The tribocorrosion tests were performed under a single set of mechanical and electrochemical conditions, which enables controlled comparison but does not represent the full range of service environments these coatings may encounter. The electrochemical response was monitored through open-circuit potential, a technique well suited for capturing depassivation and repassivation during sliding, though it does not provide quantitative corrosion kinetics. At the same time, it should be noted that dry sliding serves only as a qualitative upper-bound reference for mechanical wear and does not replicate the lubrication, thermal behavior, or interfacial chemistry present during tribocorrosion. As such, the comparison provides mechanistic context rather than a direct decomposition of mechanical and electrochemical contributions. Finally, the tests were designed to characterize the initial tribocorrosion response of the two hard coatings rather than to support full statistical modeling of variability or long-term durability.

## 4. Conclusions

In this research, both boride and niobium carbide (NbC) coatings were successfully synthesized on Vanadis 6 cold-work tool steel using a thermochemical powder-pack diffusion (TCD) technique. The coatings were systematically characterized in terms of microstructure, microhardness, frictional behavior, wear resistance, and tribocorrosion performance. Based on the experimental findings, the following conclusions can be drawn.

- Both borided and NbC coatings were deposited on Vanadis 6 steel via the TCD method. The borided layer exhibited a thickness of approximately 90–100 μm, while the NbC coating measured around 10–15 μm. The borided samples achieved a peak surface hardness of 2000 HV0.1, whereas NbC coatings reached hardness value of 1550 HV0.1.
- Under dry sliding conditions, both coatings produced a measurable improvement in frictional behavior, lowering the mean coefficient of friction by approximately 17% relative to the uncoated steel. In terms of material loss, the borided surface exhibited a 60% reduction in wear volume, while the NbC-coated surface showed a 32% reduction compared with the uncoated surface.
- Analysis of the worn surfaces after dry sliding showed that the uncoated steel experienced pronounced abrasive wear together with extensive oxidation, whereas the coated specimens primarily displayed oxidation-assisted adhesive wear.
- Open-circuit potential measurements showed that all coated samples exhibited higher corrosion resistance than the uncoated steel. During tribocorrosion testing in Na-tetraborate solution, both coatings had pseudo passive behavior. In contrast, testing in NaCl and NaOH led to a marked increase in corrosion activity during sliding.
- All samples subjected to tribocorrosion showed evidence of oxidation driven by mechanical wear, independent of the coating type or the electrolyte used.
- The uncoated and borided specimens predominantly formed magnetite ($Fe_3O_4$), and hematite ($\alpha$-$Fe_2O_3$), indicating a mixed oxide layer. In contrast, the NbC-coated specimen exhibited goethite ($\alpha$-FeOOH) corrosion products.
- Overall, the study shows that boride and NbC coatings provide effective surface protection for Vanadis 6 tool steel. Both coatings improved resistance to mechanical wear and corrosion-assisted degradation, confirming their suitability for demanding contact conditions. In addition, sodium tetraborate emerged as a stable and reliable electrolyte for tribocorrosion testing of non-passive alloy systems.
- Although both coatings enhanced the tribocorrosion performance of Vanadis 6 steel, the NbC layer demonstrated superior corrosion resistance even at significantly lower thickness, while the borided layer provided the greatest improvement in wear resistance due to its higher hardness and load-bearing capacity. These results indicate that NbC coating can serve as a viable alternative to boriding when improved corrosion behavior and material toughness are required, whereas boriding remains advantageous in applications dominated by mechanical wear.

## CRediT authorship contribution statement

**Venu Yarasu:** Conceptualization, Data curation, Formal analysis, Investigation, Methodology, Validation, Visualization, Writing –

original draft. **Bojan Podgornik:** Funding acquisition, Project administration, Resources, Supervision, Writing – review & editing. **Tadeja Kosec:** Conceptualization, Data curation, Methodology, Supervision, Writing – review & editing. **Peter Jurči:** Conceptualization, Funding acquisition, Methodology, Project administration, Resources, Supervision, Writing – review & editing. **Ali Günen:** Conceptualization, Methodology, Resources, Writing – review & editing. **Peter Orihel:** Conceptualization, Methodology. **Sabri Alkan:** Writing – review & editing.

## Declaration of competing interest

The authors declare that they have no known competing financial interests or personal relationships that could have appeared to influence the work reported in this paper.

## Acknowledgements

The authors acknowledge the technical and scientific staff assistance of Institute of Metals and Technology, Slovenia. The authors acknowledge the financial support from the Slovenian Research Agency (research core funding No. P2-0050 and P2-0273).

## Data availability

Data will be made available on request.

## References

[1] Bartkowska, A., Swadźba, R., Popławski, M., Bartkowski, D., 2016. Microstructure, microhardness, phase analysis and chemical composition of laser remelted FeB-Fe2B surface layers produced on Vanadis-6 steel. Opt. Laser Technol. 86, 115–125. https://doi.org/10.1016/j.optlastec.2016.07.010.

[2] Tobola, D., Kania, B., 2018. Phase composition and stress state in the surface layers of burnished and gas nitrided Sverker 21 and Vanadis 6 tool steels. Surf. Coat. Technol. 353, 105–115. https://doi.org/10.1016/j.surfcoat.2018.08.055.

[3] Jurči, P., Dománková, M., Hudáková, M., Ptačinová, J., Pašák, M., Palček, P., 2017. Characterization of microstructure and tempering response of conventionally quenched, short- and long-time sub-zero treated PM Vanadis 6 ledeburitic tool steel. Mater. Charact. 134, 398–415. https://doi.org/10.1016/j.matchar.2017.10.029.

[4] Yarasu, V., Jurci, P., Hornik, J., Krum, S., 2022. Optimization of cryogenic treatment to improve the tribological behavior of Vanadis 6 steel using the Taguchi and grey relation approach. J. Mater. Res. Technol. 18, 2945–2962. https://doi.org/10.1016/j.jmrt.2022.03.145.

[5] Wood, R.J.K., Lu, P., 2024. Coatings and surface modification of alloys for tribo-corrosion applications. Coatings 14, 99. https://doi.org/10.3390/coatings14010099.

[6] Soltani, R., Sohi, M.H., Ansari, M., Haghighi, A., Ghasemi, H.M., Haftlang, F., 2017. Evaluation of niobium carbide coatings produced on AISI L2 steel via thermo-reactive diffusion technique. Vacuum 146, 44–51. https://doi.org/10.1016/j.vacuum.2017.09.023.

[7] Wood, R.J.K., Wharton, J.A., 2011. Coatings for tribocorrosion protection. In: Tribocorrosion Passive Met. Coat. Elsevier, pp. 296–333. https://doi.org/10.1533/9780857093738.2.296.

[8] Akhbarizadeh, A., Amini, K., Javadpour, S., 2012. Effects of applying an external magnetic field during the deep cryogenic heat treatment on the corrosion resistance and wear behavior of 1.2080 tool steel. Mater. Des. 41, 114–123. https://doi.org/10.1016/j.matdes.2012.03.045.

[9] Hill, H., Huth, S., Weber, S., Theisen, W., 2011. Corrosion properties of a plastic mould steel with special focus on the processing route. Mater. Corros. 62, 436–443. https://doi.org/10.1002/maco.200905570.

[10] Wang, Q., 2025. Electrochemical evaluation of nanostructured coatings for corrosion protection of structural metals. Int. J. Electrochem. Sci. 20, 101214. https://doi.org/10.1016/j.ijoes.2025.101214.

[11] Zhang, L., Hong, X., Li, Z., Song, J., Yang, Z., Liu, J., Huang, J., 2025. Comprehensively evaluating and unraveling the electrical conductivity, corrosion resistance and mechanical properties of metal carbide coatings for metal bipolar plates. Mater. Today Commun. 46, 112713. https://doi.org/10.1016/j.mtcomm.2025.112713.

[12] Medvedovski, E., Jiang, J., Robertson, M., 2016. Iron boride-based thermal diffusion coatings for tribo-corrosion oil production applications. Ceram. Int. 42, 3190–3211. https://doi.org/10.1016/j.ceramint.2015.10.109.

[13] Günen, A., Soylu, B., Karakaş, Ö., 2022. Titanium carbide coating to improve surface characteristic, wear and corrosion resistance of spheroidal graphite cast irons. Surf. Coat. Technol. 437, 128280. https://doi.org/10.1016/j.surfcoat.2022.128280.

[14] Enrique Castillejo Nieto, F., Maritza Marulanda Cardona, D., 2025. Recent advances and challenges of the thermo-reactive deposition-diffusion (TRD) process for corrosion control in steels. In: Abdel Hamid, Z., Hasan Gomaa, M. (Eds.), Mater. Sci. IntechOpen. https://doi.org/10.5772/intechopen.1010062.

[15] Karakaş, M.S., 2020. Tribocorrosion behavior of surface-modified AISI D2 steel. Surf. Coat. Technol. 394, 125884. https://doi.org/10.1016/j.surfcoat.2020.125884.

[16] Sudarshan, T.S. (Ed.), 2015. Surface Modification Technologies XXVIII: Proceedings of the Twenty Eighth International Conference on Surface Modification Technologies ; Held at Tampere University of Technology, Tampere. Finland, June 16 - 18, 2014, 1. print, Valardocs, Chennai.

[17] Keddam, M., Hudáková, M., Ptačinová, J., Moravčík, R., Gogola, P., Gabalcová, Z., Jurči, P., 2021. Characterization of boronized layers on Vanadis 6 tool steel. Surf. Eng. 37, 445–454. https://doi.org/10.1080/02670844.2020.1781377.

[18] Günen, A., Altınay, Y., Sabun, Ş., Alkan, S., 2024. Effect of the incorporating of refractory NbC precipitates in intermetallic iron-aluminide coatings on corrosion and high-temperature oxidation behavior. Surf. Coat. Technol. 483, 130774. https://doi.org/10.1016/j.surfcoat.2024.130774.

[19] Çakir, M.V., 2022. A comparative study on tribocorrosion wear behavior of boride and vanadium carbide coatings produced by TRD on AISI D2 steel. Protect. Met. Phys. Chem. Surface 58, 562–573. https://doi.org/10.1134/S2070205122030042.

[20] Günen, A., Açıkgöz, H.H., Karahan, İ.H., 2023. Niobium carbide coatings grown on cold work tool steel AISI D3 by thermomechanical processing: characterization, wear and corrosion behaviors. Protect. Met. Phys. Chem. Surface 59, 648–670. https://doi.org/10.1134/S207020512370065X.

[21] Panda, J.N., Wong, B.C., Medvedovski, E., Egberts, P., 2021. Enhancement of tribo-corrosion performance of carbon steel through boronizing and BN-based coatings. Tribol. Int. 153, 106666. https://doi.org/10.1016/j.triboint.2020.106666.

[22] Medvedovski, E., Leal Mendoza, G., Vargas, G., 2021. Influence of boronizing on steel performance under erosion-abrasion-corrosion conditions simulating downhole oil production. Corros. Mater. Degrad. 2, 293–324. https://doi.org/10.3390/cmd2020016.

[23] Alkan, S., Günen, A., Gülen, M., Gök, M.S., 2024. Effect of boriding on tribocorrosion behaviour of HSLA offshore mooring chain steel. Surf. Coat. Technol. 476, 130276. https://doi.org/10.1016/j.surfcoat.2023.130276.

[24] Monticelli, C., Balbo, A., Zucchi, F., 2011. Corrosion and tribocorrosion behaviour of thermally sprayed ceramic coatings on steel. Surf. Coat. Technol. 205, 3683–3691. https://doi.org/10.1016/j.surfcoat.2011.01.023.

[25] Carquigny, S., Takadoum, J., Ivanescu, S., 2019. Corrosion and tribocorrosion study of 316L steel, Ti–6Al–4V and Ti–10Zr–10Nb–5Ta. Tribol. Mater. Surf. Interfaces 13, 112–119. https://doi.org/10.1080/17515831.2019.1596625.

[26] Dantas, A., Dantas, R., Cipriano, G.P., De Jesus, A., Lesiuk, G., Fonseca, C., Moreira, P., Correia, J.A.F.O., 2024. A methodology to evaluate seawater corrosion on quasi-static tensile properties of a structural steel. Eng. Fail. Anal. 164, 108613. https://doi.org/10.1016/j.engfailanal.2024.108613.

[27] Sherif, E.-S., 2014. A comparative study on the electrochemical corrosion behavior of iron and X-65 steel in 4.0 wt % sodium chloride solution after different exposure intervals. Molecules 19, 9962–9974. https://doi.org/10.3390/molecules19079962.

[28] Wood, R.J.K., 2007. Tribo-corrosion of coatings: a review. J. Phys. Appl. Phys. 40, 5502–5521. https://doi.org/10.1088/0022-3727/40/18/S10.

[29] Fan, H., Li, F., Huang, H., Yang, J., Zeng, D., Liu, J., Mou, H., 2022. pH graded lignin obtained from the by-product of extraction xylan as an adsorbent. Ind. Crops Prod. 184, 114967. https://doi.org/10.1016/j.indcrop.2022.114967.

[30] Yang, C., Meng, X., Li, X., Li, Z., Yan, H., Wu, L., Cao, F., 2023. Effect of electrolyte composition on corrosion behavior and tribological performance of plasma electrolytic oxidized TC4 alloy. Trans. Nonferrous Met. Soc. China 33, 141–156. https://doi.org/10.1016/S1003-6326(22)66096-5.

[31] Berradja, A., 2018. A tribo-electrochemical investigation of degradation processes in metallic glasses. In: Huang, H. (Ed.), Met. Glas. - Prop. Process. InTech. https://doi.org/10.5772/intechopen.79387.

[32] Tan, L., Wang, Z., Ma, Y., 2021. Tribocorrosion behavior and degradation mechanism of 316L stainless steel in typical corrosive media. Acta Metall. Sin. Engl. Lett. 34, 813–824. https://doi.org/10.1007/s40195-020-01182-1.

[33] Mohamed, A., Martin, U., Visco Jr., D.P., Townsend, T., Bastidas, D.M., 2023. Interphase corrosion inhibition mechanism of sodium borate on carbon steel rebars in simulated concrete pore solution. Constr. Build. Mater. 408, 133763. https://doi.org/10.1016/j.conbuildmat.2023.133763.

[34] The inhibition effect of sodium tetraborate on the corrosion of steel in KOH media. Int. J. Corros. Scale Inhib. 7, 2018. https://doi.org/10.17675/2305-6894-2018-7-3-9.

[35] Cui, J., Yuan, W., Pei, Y., 2019. Corrosion resistance of carbon steel under an aerobic acidic condition in the presence of borate as corrosion inhibitor, Anti-Corros. Methods Mater 66, 88–100. https://doi.org/10.1108/ACMM-04-2018-1918.

[36] Jurči, P., Orihel, P., Keddam, M., Vretenár, V., Maťko, M., 2025. Boride layers on high-carbon high-chromium tool steels: microstructure-mechanical properties relationship. J. Mater. Res. Technol. 39, 5808–5821. https://doi.org/10.1016/j.jmrt.2025.10.154.

[37] Molaei, M., Fattah-Alhosseini, A., Keshavarz, M.K., 2019. Influence of different sodium-based additives on corrosion resistance of PEO coatings on pure Ti. J. Asian Ceram. Soc. 7, 247–255. https://doi.org/10.1080/21870764.2019.1604609.

[38] Andreasen, J.L., Bay, N., De Chiffre, L., 1998. Quantification of galling in sheet metal forming by surface topography characterisation. Int. J. Mach. Tool Manufact. 38, 503–510. https://doi.org/10.1016/S0890-6955(97)00095-3.

[39] Mousavi, A., 2020. A Novel Approach Towards a Lubricant-free Deep Drawing Process via macro-structured Tools. TUDpress, Dresden.
[40] Yapici, A., Aydin, S.E., Koc, V., Kanca, E., Yildiz, M., 2019. Wear behavior of borided AISI D2 steel under linear reciprocating sliding conditions. Protect. Met. Phys. Chem. Surface 55, 341–351. https://doi.org/10.1134/S207020511902028X.
[41] Reséndiz-Calderón, C.D., Cao-Romero-Gallegos, J.A., Farfan-Cabrera, L.I., Campos-Silva, I., Soriano-Vargas, O., 2024. Influence of boriding on the tribological behavior of AISI D2 tool steel for dry deep drawing of stainless steel and aluminum. Surf. Coat. Technol. 484, 130832. https://doi.org/10.1016/j.surfcoat.2024.130832.
[42] Castillejo, F.E., Marulanda, D.M., Olaya, J.J., Alfonso, J.E., 2014. Wear and corrosion resistance of niobium–chromium carbide coatings on AISI D2 produced through TRD. Surf. Coat. Technol. 254, 104–111. https://doi.org/10.1016/j.surfcoat.2014.05.069.
[43] Mariani, F.E., Lombardi, A.N., Casteletti, L.C., 2023. Tribological evaluation of NbC and VC layers produced by thermo-reactive diffusion treatment in ductile cast irons with varying composition. J. Mater. Eng. Perform. 32, 5421–5434. https://doi.org/10.1007/s11665-022-07495-9.
[44] Morón, R.C., Hernández-Onofre, I., Contla-Pacheco, A.D., Bravo-Bárcenas, D., Campos-Silva, I., 2020. Friction and reciprocating wear behavior of borided AISI H13 steel under dry and lubricated conditions. J. Mater. Eng. Perform. 29, 4529–4540. https://doi.org/10.1007/s11665-020-04957-w.
[45] Günen, A., Açikgöz, H.H., Çavdar, F., Karahan, İsH., 2023. A response surface study on the grown behavior and some mechanical properties of niobium carbide coatings. Surf. Rev. Lett. 30, 2350058. https://doi.org/10.1142/S0218625X23500580.
[46] Liao, Y., Zhang, F., Pan, X., Li, K., Zhou, Y., Wu, S., 2023. A comparative study on tribological behavior of Al2O3, AlN, Si3N4 and ZrO2 ceramics sliding against polycrystalline diamond ball. Wear 530–531, 205067. https://doi.org/10.1016/j.wear.2023.205067.
[47] Orihel, P., Jurči, P., Pašák, M., 2024. Evaluation of Fracture Toughness of Boride Layers on High Chromium Steels, pp. 258–263. https://doi.org/10.37904/metal.2024.4890.
[48] Üçisik, A.H., Bindal, C., 1997. Fracture toughness of boride formed on low-alloy steels. Surf. Coat. Technol. 94–95, 561–565. https://doi.org/10.1016/S0257-8972(97)00466-0.
[49] Zhao, Z., Hui, P., Liu, F., Xu, Y., Zhong, L., Zhao, M., 2020. Fabrication of niobium carbide coating on niobium by interstitial carburization. Int. J. Refract. Met. Hard Mater. 88, 105187. https://doi.org/10.1016/j.ijrmhm.2020.105187.
[50] Da Costa Aichholz, S.A., Sostag Meruvia, M., Soares Júnior, P.C., Torres, R.D., 2018. Tribocorrosion behavior of boronized AISI 4140 steel. Surf. Coat. Technol. 352, 265–272. https://doi.org/10.1016/j.surfcoat.2018.07.101.
[51] Tait, W.S., 1994. An Introduction to Electrochemical Corrosion Testing for Practicing Engineers and Scientists. PairODocs Publ, Racine, Wisc.
[52] Dubois, F., Mendibide, C., Pagnier, T., Perrard, F., Duret, C., 2008. Raman mapping of corrosion products formed onto spring steels during salt spray experiments. A correlation between the scale composition and the corrosion resistance. Corros. Sci. 50, 3401–3409. https://doi.org/10.1016/j.corsci.2008.09.027.